Film rupture in the diffuse interface model coupled to hydrodynamics

Uwe Thiele and Manuel G. Velarde
Instituto Pluridisciplinar, Universidad Complutense, Paseo Juan XXIII, 1, 28040 Madrid, Spain

Kai Neuffer
Instituto Pluridisciplinar, Universidad Complutense, Paseo Juan XXIII, 1, 28040 Madrid, Spain
and Lehrstuhl für Statistische Physik und Nichtlineare Dynamik, BTU-Cottbus, Erich-Weinert-Strasse 1, 03046 Cottbus, Germany

Yves Pomeau
Instituto Pluridisciplinar, Universidad Complutense, Paseo Juan XXIII, 1, 28040 Madrid, Spain;
Laboratoire de Physique Statistique de l'Ecole Normale Supérieure, associè au CNRS,
24 Rue Lhomond, 75231 Paris Cedex 05, France;
and Laboratoire ASCI, Bâtiment 506, 91405 Orsay Cedex, France

(Received 21 December 2000; revised manuscript received 30 April 2001; published 10 August 2001)

The process of dewetting of a thin liquid film is usually described using a long-wave approximation yielding a single evolution equation for the film thickness. This equation incorporates an additional pressure term—the disjoining pressure—accounting for the molecular forces. Recently a disjoining pressure was derived coupling hydrodynamics to the diffuse interface model [L. M. Pismen and Y. Pomeau, Phys. Rev. E **62**, 2480 (2000)]. Using the resulting evolution equation as a generic example for the evolution of unstable thin films, we examine the thickness ranges for linear instability and metastability for flat films, the families of stationary periodic and localized solutions, and their linear stability. The results are compared to simulations of the nonlinear time evolution. From this we conclude that, within the linearly unstable thickness range, there exists a well defined subrange where finite perturbations are crucial for the time evolution and the resulting structures. In the remainder of the linearly unstable thickness range the resulting structures are controlled by the fastest flat film mode assumed up to now for the entire linearly unstable thickness range. Finally, the implications for other forms of disjoining pressure in dewetting and for spinodal decomposition are discussed.

DOI: 10.1103/PhysRevE.64.031602 PACS number(s): 68.15.+e, 68.55.−a, 47.20.Ma, 64.70.−p

I. INTRODUCTION

The stability of thin liquid films on solid substrates is of interest in applications such as coating or drying processes. Destabilizing influences leading to film rupture can arise from gradients in the surface tension caused by a spatial variation of temperature or surfactant concentration fields, by evaporation, or by molecular forces. The latter forces are especially important for very thin films with thicknesses smaller than 100 nm. The rupture process due to molecular forces, and hence dewetting, is studied either to understand how to keep thin films stable [1] or how to produce structured thin films in a controlled manner [2].

Dewetting proceeds by the formation of holes in unstable films. Subsequently the lateral expansion of the holes results in the formation of a polygonal network of liquid rims or ensembles of liquid drops [3,4]. Experimental and theoretical investigations focus on all aspects of the process: the initial rupture of the film [5,1,6], the growth process of single holes [7,8], the evolution and the final state of the overall pattern [4,2,9,10], and instabilities during hole growth [11].

For the film rupture the two widely discussed mechanisms are surface instability and heterogeneous nucleation due to defects. They occur in the range of metastable and linearly unstable film thicknesses, respectively [1,4,9,12–15,6]. Different procedures have been proposed to distinguish the mechanisms through an analysis of the final hole pattern. On the one hand, the change of hole density with film thickness is compared with the dependence of wavelength on thickness taken from the linear stability analysis [4,16]. On the other hand, ordered and disordered arrangements of holes are found to be caused by instability and nucleation, respectively [12,9,14].

To describe the dewetting process one takes advantage of the disparity of the length scales, film thickness, and lateral changes in the film profile, that allows the use of the long-wave or lubrication approximation of Stokes equations [17]. The resulting nonlinear evolution equation for the film thickness is formally similar to the Cahn-Hillard equation that describes the spinodal decomposition of a binary mixture [18]. Therefore, the rupture due to the surface instability is also called ''spinodal dewetting'' [19].

The possibly destabilizing molecular forces are included in the thickness evolution equation as an additional pressure term, the so-called disjoining pressure first introduced by Derjaguin and co-workers [20,21]. Depending on the particular problem treated, the disjoining pressure may incorporate van der Waals, electrostatic, and structural interaction terms [22–25]. Every term of the disjoining pressure acts on its specific thickness scale, and can be stabilizing or destabilizing. The large number of possible combinations can be roughly ordered by some of the global features of the dependence of the disjoining pressure on film thickness, such as the behavior for small and large film thicknesses, and number of maxima or minima. Standard choices normally include short- and long-range components that can be destabilizing

or stabilizing. Their combination gives four types of disjoining pressure [26,27] that have been used to study the two- and three-dimensional evolution of unstable films [28–32]. A common shortcoming of all the used pressures known to the authors are the singularities arising when the film thickness goes to zero.

Recently, Pismen and Pomeau combined the long-wave approximation for thin films with a diffuse interface description for the surface of the liquid, to derive a disjoining pressure that does not contain divergencies for vanishing film thickness [33]. First they discussed the vertical density profile for a liquid in a flat horizontal layer of fluid incorporating a smooth but nevertheless relatively sharp density transition between fluid and gas, and the density variation close to the solid substrate due to molecular interactions that enter into the calculation via the boundary condition for the fluid density at the substrate. Then they combined the obtained density profile with the Stokes equation in the long-wave approximation to account for dynamic situations. The arising film thickness equation has the typical form of a thin film equation with disjoining pressure [17], where the disjoining pressure now results from diffuse interface theory. We use the film thickness equation from Ref. [33] to perform a detailed analysis of the competing mechanisms leading to the rupture of a thin liquid film. By ''rupture'' here we mean not true rupture leading to patches of dry substrate but the formation of holes with a very thin remaining film, as in a precursor film model [34]. On the one hand, the analysis aims at generic results for film rupture on a horizontal substrate under the influence of destabilizing short-range and stabilizing long-range interactions also applicable to other disjoining pressures. On the other hand, it also serves as a key study for later analyses of sliding drops on an inclined plane or with surface tension gradient forces.

We begin with a thin film evolution equation, discuss the scaling used, introduce a Lyapunov function (free energy potential), and proceed with the derivation of the stationary equation (Sec. II). In the following we discuss stability, metastability, and linear instability for a flat or homogeneous film (Sec. III), and calculate the families of stationary inhomogeneous (periodic and localized) solutions in the different parameter ranges (Sec. IV). For particular parameter values, analytical solutions are given. The linear stability analysis of these solutions (Sec. V) allows us to formulate a hypothesis on their significance in the evolution process that is checked by direct integration of the time evolution equation for linearly unstable thin films (Sec. VI). We make a distinction between two thickness subranges within the linearly unstable thickness range, where a qualitatively different behavior is predicted during structure formation: (A) a nucleation-dominated subrange, where initial small-scale finite disturbances determine the final structure, hence overcoming the fastest flat film mode; and (B) and instability-dominated subrange, where the fastest flat film mode overcomes the finite perturbations. Finally, in Sec. VII we discuss the applicability of our main results to thin liquid films subject to various disjoining pressures formally similar to the one studied here, as, for example, the combination of a destabilizing short-range polar and a stabilizing long-range apolar interaction as

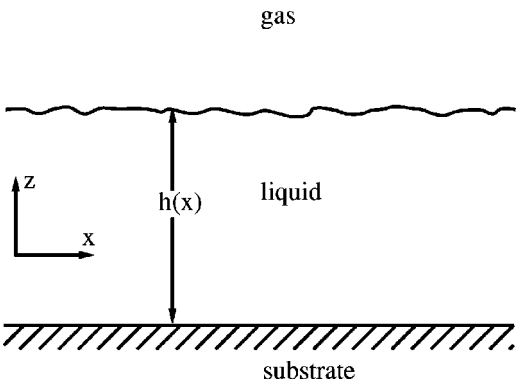

FIG. 1. Sketch of the two-dimensional geometry.

used in Refs. [11,26,28,30,31,35,36], and to the spinodal decomposition of binary mixtures by clarifying in which way we have extended earlier results on solution types and their stability [37–40].

II. FILM THICKNESS EVOLUTION EQUATION

Using a diffuse interface model and the long-wave or lubrication approximation the film thickness evolution equation for a thin liquid film on a solid substrate was derived in Ref. [33]. For a two-dimensional geometry, as sketched in Fig. 1, it writes

$$\partial_t h = -\partial_x\{Q(h)\partial_x[\gamma\partial_{xx}h - \partial_h f(h,a)]\}, \tag{1}$$

where h denotes the film thickness, and $Q(h)=h^3/3\eta$ the mobility factor due to the assumed Poiseuille flow. $\gamma\partial_{xx}h$ represents the Laplace or curvature pressure, and

$$\partial_h f(h,a) = \kappa M(h,a) + \rho g h = \frac{2\kappa}{a} e^{-h/l}\left(1 - \frac{1}{a}e^{-h/l}\right) + \rho g h \tag{2}$$

is an additional pressure term corresponding to the free energy $f(h,a)$. g is the gravitational acceleration, and ρ, γ, and η are the respective density, surface tension, and viscosity of the liquid. $\Pi(h) = -\kappa M(h,a)$ is the disjoining pressure arising from diffuse interface theory, the constant κ has the dimension of a spreading coefficient per length, a is a small dimensionless positive parameter describing the wetting, properties in the regime of partial wetting and l is the length scale of the diffuse interface [33]. The functional form of $M(h,a)$ (scaled as explained below) can be seen in Fig. 2. $\rho g h$ is the hydrostatic pressure. Subscripts t, x, and h denote the corresponding partial derivatives.

A. Scaling

To introduce dimensionless quantities (with tilde), suitable new scales are used:

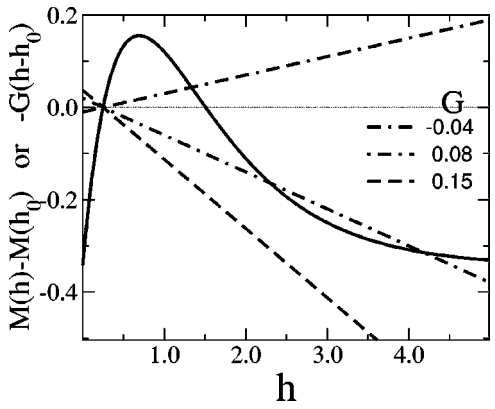

FIG. 2. Fixed points of the dynamical system represented as crossings of the curves $M(h)-M(h_0)$ (solid line) and $-G(h-h_0)$ (broken lines) at $h_0=1/4$ and different G.

$$t=\frac{3\eta\gamma_{\sim}}{\kappa^2 l}\tilde{t},$$
$$h=l\tilde{h}, \tag{3}$$
$$x=\sqrt{\frac{l\gamma}{\kappa}}\tilde{x}.$$

The ratio $\kappa l/\gamma$ is $O(a^2)$ [33], i.e., the scale in the x direction is l/a. Expecting no confusion from the reader after dropping the tildes, we find

$$\partial_t h=-\partial_x\{h^3\partial_x[\partial_{xx}h-M(h,a)-Gh]\} \tag{4}$$

where

$$G=\frac{l\rho g}{\kappa} \tag{5}$$

gives the ratio between gravitation and molecular interactions with values always taken to be positive. We will see that even if G is very small we cannot drop it, because it crucially influences the behavior of the solution of the system; the problem is singular at $G=0$. The form of $M(h,a)$ allows us to transfer the constant a into the mobility factor Q by the transformation $h^*=h+\ln a$. After dropping the star, and once more expecting no confusion in the reader, we find

$$M(h)=2e^{-h}(1-e^{-h}), \tag{6}$$

while the evolution equation (1) becomes

$$\partial_t h=-\partial_x\{(h-\ln a)^3\partial_x[\partial_{xx}h-\partial_h f(h)]\}, \tag{7}$$

with

$$\partial_h f(h)=M(h)+Gh. \tag{8}$$

From now on we will use the general form $\partial_h f(h)$, introducing the example treated here only in the final stage of calculations. In this way all derivations can be used easily whatever the particular disjoining pressure used [26,28,30,31,35,36,41].

B. Lyapunov functional

At different stages of our investigation we need a valid measure for the energy that can be assigned to a given film thickness profile, $h(x,t)$. For this purpose, following, for example, Refs. [39,42,19], we introduce a semidefinite positive functional

$$F(h)=\int\left[\frac{1}{2}(\partial_x h)^2+f(h)-C_1(h-\overline{h})\right]dx, \tag{9}$$

which we shall show is a Lyapunov functional. $\overline{h}$ is the mean film thickness, and here C_1 is the Lagrange multiplier corresponding to material conservation needed when comparing different stationary solutions for the same liquid volume. To show that $F(h)$ is a Lyapunov functional, we have to prove that its functional derivative is semidefinite negative. We write the evolution equation (7) as

$$\partial_t h=\partial_x\left(Q(h)\partial_x\frac{\delta F}{\delta h}\right), \tag{10}$$

with $Q(h)=(h-\ln a)^3$, and δ denoting functional variation. Multiplying Eq. (10) by $\delta F/\delta h$, and integrating with respect to x, gives, after integration by parts, the total time derivative of F:

$$\frac{dF}{dt}=-\int Q(h)\left(\partial_x\frac{\delta F}{\delta h}\right)^2 dx. \tag{11}$$

Studying only situations with positive physical film thickness, $h-\ln a$, the derivative dF/dt is always negative, and so F is a good choice for a Lyapunov or energy functional. We will further call it ''energy,'' for short, and use it to compare stationary solutions to determine their absolute stability and measure their time evolution in the numerical integration of Eq. (7).

C. Stationary equation

To study stationary and especially homogeneous or flat film solutions, we set $\partial_t h=0$ and integrate Eq. (7), yielding

$$0=\partial_{xxx}h-(\partial_{hh}f(h))\partial_x h+\frac{C_0}{Q(h)}. \tag{12}$$

We are looking for bounded solutions of three types: (a) periodic solutions, (b) localized solutions, and (c) flat film solutions. For (a) the reflection symmetry with respect to the extrema of the solutions implies $C_0=0$. The same follows for (b) and (c), because there all x derivatives vanish at infinity. A second integration yields

$$0=\partial_{xx}h(x)-\partial_h f(h)+C_1. \tag{13}$$

The constant C_1 accounts for external conditions like chemical potential, vapor pressure, or mass conservation. Regard-

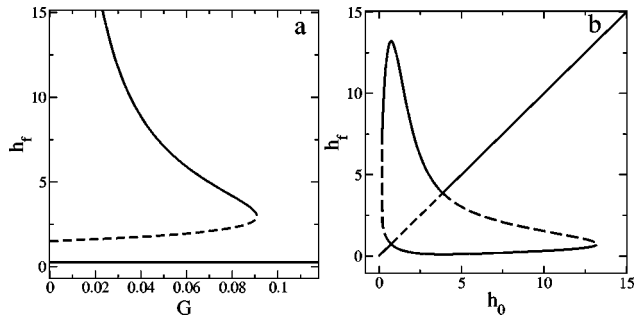

FIG. 3. Bifurcation diagram for (a) fixed $h_0=1/4$, and (b) fixed $G=0.04$ showing flat film solutions according to the values G and h_0, respectively. Solid and dashed lines correspond, respectively, to linearly stable (saddle) and linearly unstable (center) ranges.

ing the latter, the choice $C_1=\partial_h f(h_0)=M(h_0)+Gh_0$ ensures a flat film solution of Eq. (13), $h(x)=h_0$. Using the same $C_1(h_0)$ for localized solutions, h_0 is the thickness at infinity, h_∞. For periodic solutions, h_0 is the thickness at the inflection point of the respective profile. Its difference from the thickness at the maximum or minimum of the period is a measure of the curvature at the maximum and minimum, respectively. Note that Eq. (13) also follows from the minimization of the energy functional [Eq. (9)], as expected. Later we will compute periodic solutions of Eq. (13), and parametrize them by their mean film thickness, $\overline{h}=(1/p)\int_0^p h(x)dx$, and period, p. Before embarking on this, in Sec. III we study the flat film solutions of Eq. (13) and their stability.

III. HOMOGENEOUS OR UNIFORM SOLUTIONS

A chosen h_0 is by construction the thickness of a flat film solution or fixed point of Eq. (13). Due to the nonlinear relation $C_1(h_0)$, given the constant C_1 by the choice of h_0, other flat film solutions $h(x)=h_f$ are given by

$$\partial_h f(h_f)=\partial_h f(h_0). \tag{14}$$

Here they are represented by the crossing points of the curve $M(h)-M(h_0)$ with the straight line $-G(h-h_0)$, as shown in Fig. 2. For $G>0$ one finds one or three fixed points depending on the value of G and h_0. The bifurcation points between the two regimes are characterized by $\partial_{hh}f(h_0)=\partial_h M(h)+G=0$ and Eq. (14). For $(G_c=1/4,h_c=\ln 4)$ we find a critical point characterized by Eq. (14) and $\partial_{hh}f(h_c)=\partial_{hhh}f(h_c)=0$. If $G>1/4$, there exists only the fixed point h_0. Linearizing Eq. (13) around each one of the fixed points, we find that for $\partial_{hh}f(h_f)>0$ they are saddles and for $\partial_{hh}f(h_f)<0$ centers. This corresponds to the results of the linear stability analysis for flat films as will be shown below. To illustrate the existence of different flat film solutions, we plot in Fig. 3 bifurcation diagrams for (a) fixed h_0 and (b) fixed G, respectively.

A. Linear stability of flat film solutions

To assess the linear stability of the flat films $h(x)=h_0$ we use a Fourier mode decomposition $h(x)=h_0+\epsilon\exp(\beta t+ikx)$, where β provides the linear instability growth rate and k accounts for the horizontal scale of disturbances. Linearizing the full time dependent equation (7) with this ansatz yields

$$\beta=-(h_0-\ln a)^3k^2[k^2+\partial_{hh}f(h_0)]. \tag{15}$$

The flat film is unstable for $\beta>0$, i.e., for

$$\partial_{hh}f(h_0)=-2e^{-h_0}(1-2e^{-h_0})+G<0. \tag{16}$$

Accordingly, there is a range of linearly unstable thicknesses at intermediate values,

$$h_i^d<h_0<h_i^u, \tag{17}$$

with

$$h_i^{u/d}=-\ln\left[\frac{1}{2}\left(\frac{1}{2}\mp\sqrt{\frac{1}{4}-G}\right)\right]. \tag{18}$$

For $G\ll 1$ one has $h_i^d\approx-\ln(G/2)$ and $h_i^u\approx\ln 2+G$. In the limit $G\to 0$ there is no upper limit for the instability range, as even very thick films are unstable, and hence we cannot set G to zero. As derived in Appendix A 2 close to the critical point $(G_c=1/4,h_c=\ln 4)$, Eq. (18) simplifies to $h_i^{u/d}=h_c\pm 2\sqrt{G_c-G}+O(G_c-G)$.

The critical (smallest unstable) wavelength for a given film thickness h_0 is

$$\lambda_c=\frac{2\pi}{\sqrt{-\partial_{hh}f(h_0)}}. \tag{19}$$

The thickness profile $h(x)=h_0+\epsilon\exp[ik_c(h_0)x]$ with $k_c(h_0)=\sqrt{-\partial_{hh}f(h_0)}$ is neutrally stable $(\beta=0)$, and represents a small amplitude stationary solution of Eq. (13).

The fastest growing mode has the wavelength $\lambda_m=\sqrt{2}\lambda_c$ whose growth rate is

$$\beta_m=\tfrac{1}{4}(h_0-\ln a)^3[\partial_{hh}f(h_0)]^2. \tag{20}$$

The linear stability results are indeed related to the fixed points or uniform solutions discussed in Sec. III.

B. Absolute stability of flat film solutions

A linearly stable flat film may not be absolutely stable, for it can be unstable to finite amplitude disturbances. This corresponds to subcritical instability or metastability. Only if, for a given film thickness, there is no thickness profile with smaller energy is the flat film absolutely stable. To clarify this issue further, we assume an infinitely long film of thickness h_0. Only a small part of finite length s has thickness h, to ensure that the mean film thickness is h_0. The width of the finite transition region between the two thickness levels is small compared to s, so its energy can be neglected. Now we can calculate the energy per unit length of the changed part g, using the Lyapunov functional [Eq. (9)]

$$g(h)=f(h)-C_1(h_0)h+C_1(h_0)h_0, \tag{21}$$

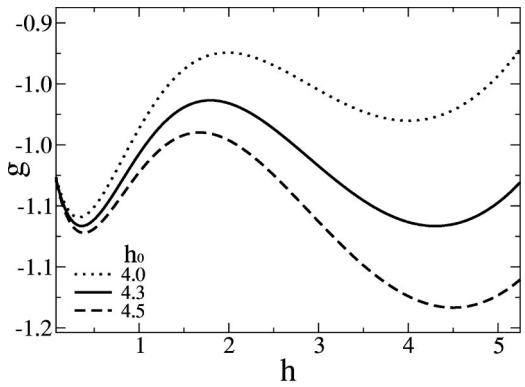

FIG. 4. The energy g for $G=0.1$ and different film thicknesses h_0. For details, see the main text.

with

$$f(h)=-e^{-h}(2-e^{-h})+Gh^2/2. \tag{22}$$

The function $g(h)-C_1(h_0)h_0$ is plotted in Fig. 4 for different values of the mean film thickness h_0, and fixed $G=0.1$. The two minima of $g(h)$ represent the lower and upper linearly stable thicknesses discussed in Sec. III A. However, only the deeper minimum corresponds to an absolutely stable film thickness, and the other is a metastable state. The maximum represents the linearly unstable thicknesses as in Sec. III A. For $0<G<G_c=1/4$ the metastable thickness range is limited by the value of h_0 where the two minima have the same depth. There exist upper and lower limits, that we denote h_m^u and h_m^d, respectively. They are characterized by

$$\begin{aligned} \partial_h f|_{h_m^u} &= \partial_h f|_{h_m^d}, \\ g(h_m^u) &= g(h_m^d). \end{aligned} \tag{23}$$

Note that the solutions of Eqs. (23) also correspond to the conditions determining the two final equilibrium film thicknesses obtained in Refs. [11,19,43] by a Maxwell construction. For low enough, albeit not vanishing $G\ll 1$, they can be determined analytically, starting from the assumptions $h_m^u \gg 1$ and $h_m^d \ll 1$. To lowest order in G, Eqs. (23) yield $h_m^d=\sqrt{G/2}+O(G)$ and $h_m^u=\sqrt{2/G}+O(G^{1/2})$ [44]. The thickness h_m^u represents the capillary length of the system determined for small G to be in physical units $\sqrt{2l\kappa/\rho g}$. Analytical approximations can also be found close to the critical point ($G_c=1/4, h_c=\ln 4$). To lowest order we have $h_m^{u/d}=h_c\pm 2\sqrt{3(G-G_c)}+O(G-G_c)$, as derived in Appendix A 2 .

Using the linear stability results of the flat film (Sec. III A) and the numerical solution of Eqs. (23) for its absolute stability, we calculate the ranges of different stability behavior in the parameter plane (G,h_0), where h_0 is the thickness of the flat film (Fig. 5). This phase diagram is valid for two- and three-dimensional film geometries. However, from now on we restrict our attention to the two-dimensional geometry, i.e., to film profiles depending on only one spatial coordinate x.

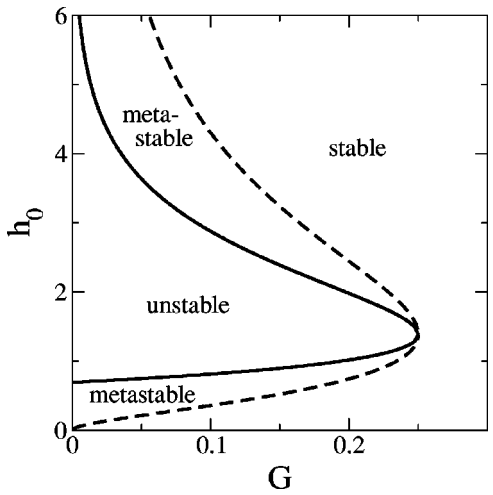

FIG. 5. The ranges for stable, metastable, and linearly unstable flat films in the parameter plane (G,h_0).

IV. INHOMOGENEOUS OR NONUNIFORM SOLUTIONS

In order to study the nonconstant solutions of Eq. (13) we multiply it by h_x and integrate:

$$\partial_x h=\sqrt{2}\sqrt{f(h)-(\partial_h f(h_0))h-C_2}. \tag{24}$$

We choose

$$C_2=f(h_m)-(\partial_h f(h_0))h_m, \tag{25}$$

where h_m is the maximal or minimal thickness for periodic solutions. For localized solutions $h_m=h_0=h_\infty$. Hence every solution is parametrized by the pair (h_0,h_m) or (C_1,C_2). Equation (25) allows us to plot the solutions in the phase plane (h,h_x). The explicit solutions $h(x)$ can be obtained by numerical integration, but for certain parameter ranges an analytical result has been obtained (see the Appendix).

In the parameter range where only one fixed point exists, there are no solutions bounded in h beside the trivial one $h(x)=h_0$. However, in a range allowing for three fixed points, three qualitatively different phase portraits can be observed, as shown on the left sides of Fig. 6(a)–6(c). We call the phase portraits the (a) drop, (b) front, and (c) hole regimes. In the hole (drop) regime one finds, in addition to periodic solutions an homoclinic solution with the lowest (highest) fixed point, representing a localized hole (drop) in an infinitely extended flat film [shown on the right sides of Figs. 6(a) and 6(c)]. These localized profiles can be found in a continuous range of the parameter plane (G,h), corresponding exactly to the metastable range for flat films in Fig. 5.

In the front regime, in addition to periodic solutions, one also finds a heteroclinic solution that connects the lowest and highest fixed points, thus representing a localized front or kink solution that connects two infinitely extended flat films of thicknesses, h_m^d and h_m^u [the right side of Fig. 6(b)]. This profile exists only for a single line in the parameter plane, identical to the border between metastable and stable flat films, as given by Eq. (23) and shown in Fig. 5. For small G

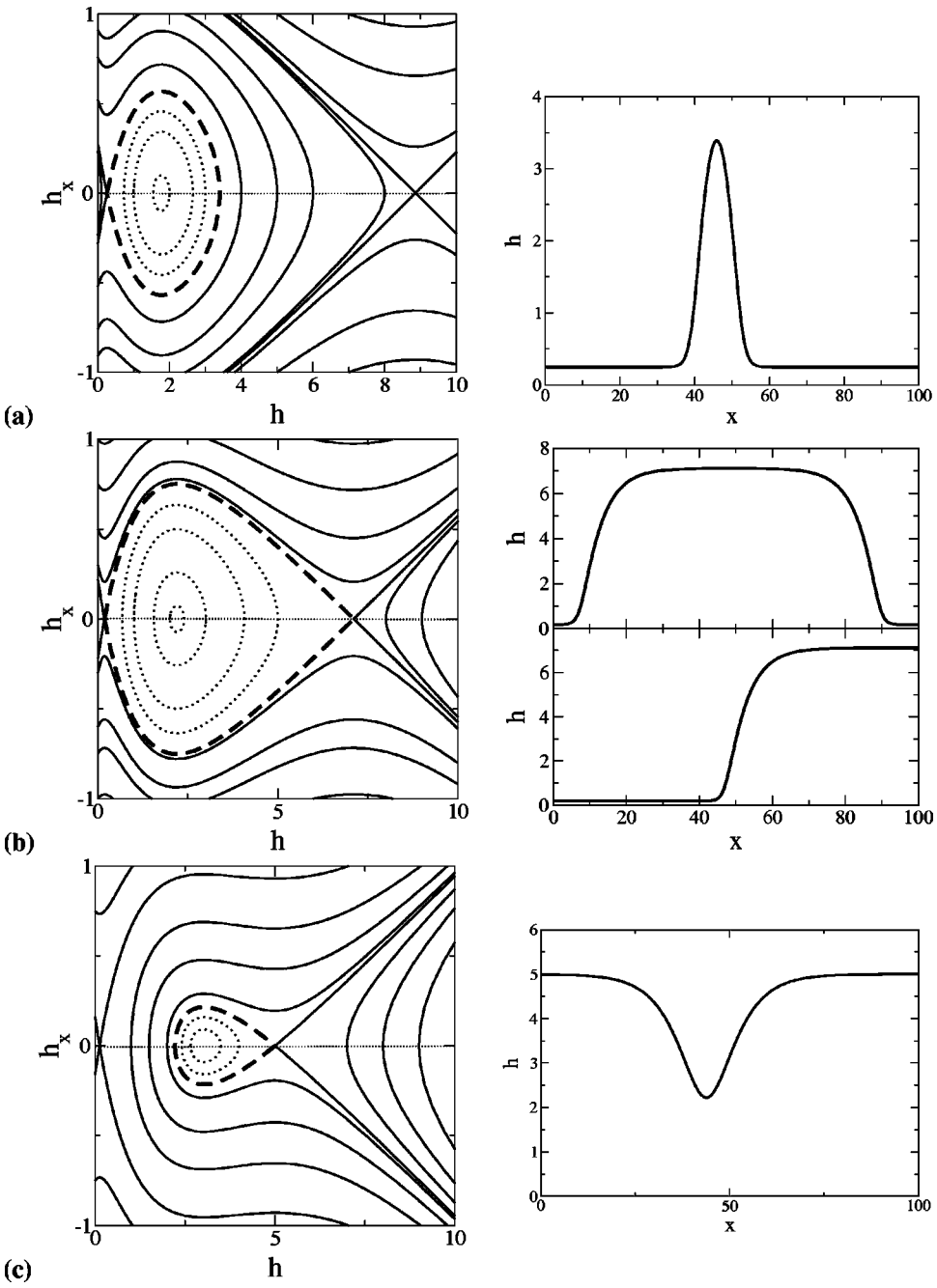

FIG. 6. Left: the phase planes (h,h_x) for different values of h_0 for $G=0.04$ showing the regimes of (a) drop, $h_0=1/4$; (b) front, $h_0=0.183086074$; and (c) hole, $h_0=5.0$. The solid, dashed, and dotted lines represent, respectively, unbound, localized, and periodic solutions. Right: Shown are the respective localized solutions: (a) homoclinic drop, (b) heteroclinic front and (c) homoclinic hole. The upper part of (b) shows a flat (pancake) drop, i.e., a periodic solution located close to the two heteroclinics in the phase plane.

the equilibrium contact angle θ_E, defined as h_x at the inflection point of the front, $h_0=-\ln\sqrt{G/2}$, is calculated to be $\theta_E=\sqrt{2}(1-\sqrt{G/2})+O(G)$. For $G=0$ the angle reduces to $\theta_E=\sqrt{2}$, the value discussed in Ref. [33] in our scaling.

Similar phase portraits were already sketched in Ref. [19] for a qualitatively similar disjoining pressure, whereas the existence of periodic solutions was discussed in Ref. [25]. In Refs. [45,46] similar hole and drop solutions were found close to a first order wetting transition, and identified as critical nuclei. Our study of the energy of the solutions also supports this finding in our case.

In the following we concentrate on periodic solutions, given that the localized solutions are also periodic solutions of infinite period. To determine the role of the periodic solutions in the time evolution of unstable films for given mean film thickness $\overline{h}$ at fixed G we calculate their period, energy, and amplitude by continuation [47], starting with the small amplitude stationary solution discussed in Sec. III A for some given $\overline{h}$ and G. In addition, close to the border between linearly stable and unstable flat films and close to the critical point, we use analytical solutions derived in the Appendix A.

Within the range of mean film thicknesses that correspond to linearly unstable or metastable flat films, for all $0<G<1/4$ we may distinguish three qualitatively different families of solutions depending on the mean film thickness. Their characterization is shown in Fig. 7 for fixed $G=0.05$ for the upper part of the parameter plane $(h>h_c)$. An identical behavior is found in the lower part. We have the following:

(i) The two lowest curves in Figs. 7(a) and 7(c) and the two leftmost in Fig. 7(e). The corresponding flat film is lin-

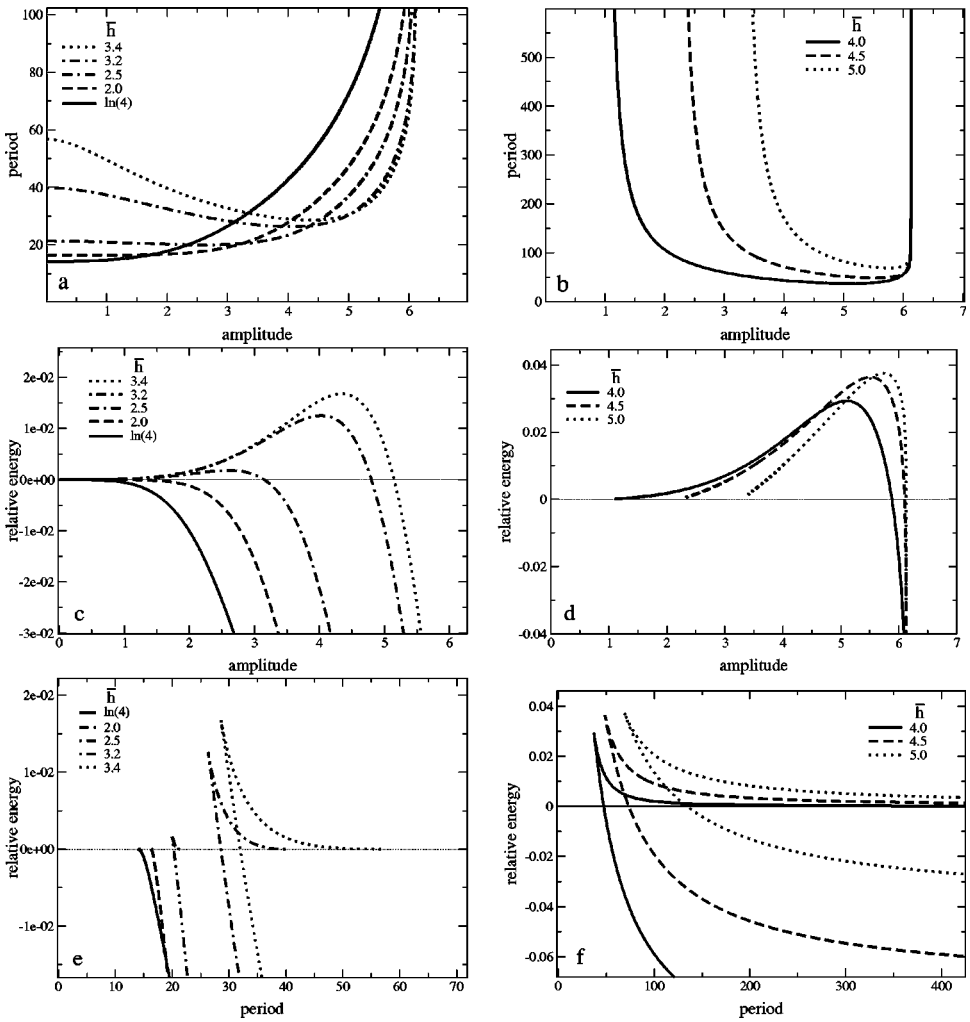

FIG. 7. Characteristics of families of periodic solutions for different mean film thickness $\bar{h}$ at fixed $G=0.05$. Shown are results for the upper part of the parameter plane in Fig. 5 ($\bar{h}>h_c$). They are qualitatively similar in the lower part. (a), (c) and (e) show the two family types in the linearly unstable $\bar{h}$ ranges called (i) and (ii) in the main text, whereas (b), (d), and (f) show the characteristics of the families in the metastable $\bar{h}$ range denotes (iii). The plots give [(a) and (b)] amplitude-period, [(c) and (d)] amplitude-energy, and [(e) and (f)] period-energy dependencies. The energy is shown relative to the corresponding flat film energy.

early unstable. There exists only one branch of stationary solutions in the period-energy plot. The period increases and the energy decreases monotonically with increasing amplitude. The energy of the periodic solutions is always lower than the corresponding energy of the flat film.

(ii) The three upper curves in Figs. 7(a) and 7(c) and the three rightmost in Fig. 7(e). The corresponding flat film is linearly unstable. There exist two branches of stationary solutions in the period-energy plot. The one with the higher energy ends at a finite period that corresponds to the wavelength of the neutrally stable solution of the linear analysis λ_c, as obtained by Eq. (19). The energy of the terminating branch is always higher than the corresponding energy of the flat film. This branch represents the nucleation solutions that have to be ''overcome'' if the film is to break into finite portions with size $p<\lambda_c$. This was checked by direct integration in time of Eq. (7) for different initial finite sinusoidal disturbances. They shrink if their amplitude is smaller then the amplitude of the corresponding nucleation solution, and grow if it is larger. The existence of the nucleation solutions may, however, also indicate that in this thickness range localized finite disturbances of a lateral extension smaller then λ_c play a significant role in the evolution of the film. Although the energy of the lower branch decreases very rapidly with increasing period, there is a very small range of periods where the flat film has the smallest energy, implying its absolute stability for systems of this size. Consequently, for this range the low-energy periodic solution is only metastable.

(iii) Curves are shown on the right side of Fig. 7. The corresponding flat film is metastable. There exist two branches of stationary solutions in the period-energy plot. Both continue towards an infinite period. The upper ones are nucleation solutions of different periods that energetically separate the lower periodic solution from the linearly stable flat film solution, i.e. perturbations with a smaller amplitude will be damped out. The single critical nucleus—the ''true'' nucleation solution—is the solution that one finds following the upper branch toward the infinite period. This is the critical drop or hole discussed for the wetting transition in Refs. [45,46]. Depending on the system size, the flat film and the lower periodic solution are absolutely stable and metastable or metastable and absolutely stable, respectively. Note that the relative energy of the solution with the smallest period changes nonmonotonically with mean film thickness.

This analysis of the stationary solutions of Eq. (1) may imply that the distinction between the instability range and the nucleation range of the film thickness generally used in the literature has to be modified to accommodate for (i) the instability range, (ii) the range of mixed behavior, and (iii) the nucleation range.

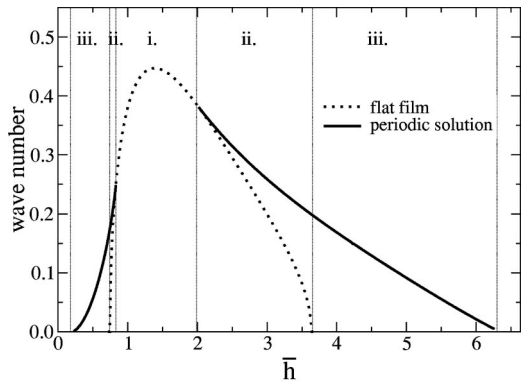

FIG. 8. Maximal wave number for nucleation solutions and the linearly unstable mode for a flat film according to the value of the mean film thickness; $G=0.05$.

To further characterize the three different ranges, in Fig. 8 we show the wave number ranges for linearly unstable flat film modes and periodic nucleation solutions according to the mean film thickness $\bar{h}$. Thereby we define a wave number for the periodic solutions in analogy to the wave number for harmonic modes as $k=2\pi/p$. From Fig. 8 one may think that the separation between (i) and (ii) is only due to finite numerical accuracy. Figure 9, however, shows that it is a true transition, as the amplitude of the nucleation solution with the highest wave number goes to zero with a power law when the film thickness approaches the border between (i) and (ii). This allows an unambiguous numerical identification of this border for all G. The resulting diagram, showing the ranges for instability, mixed behavior and nucleation, is plotted in Fig. 10. Note that the thickness at the border between instability and the mixed range does not diverge for $G\rightarrow 0$, and hence for $G\approx 0$ the prevailing range is the range of mixed behavior.

However, the study of types of solution families and their energy does not reveal what will actually happen in the physical system during the rupture process within the thickness range with mixed behavior. To clarify this issue, in the following a linear stability analysis of the periodic solutions and a direct time evolution are carried out, and the results are compared.

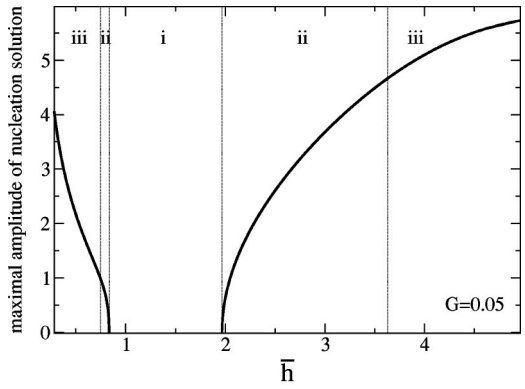

FIG. 9. Maximal amplitude of a nucleation solution according to the value of the mean film thickness; $G=0.05$.

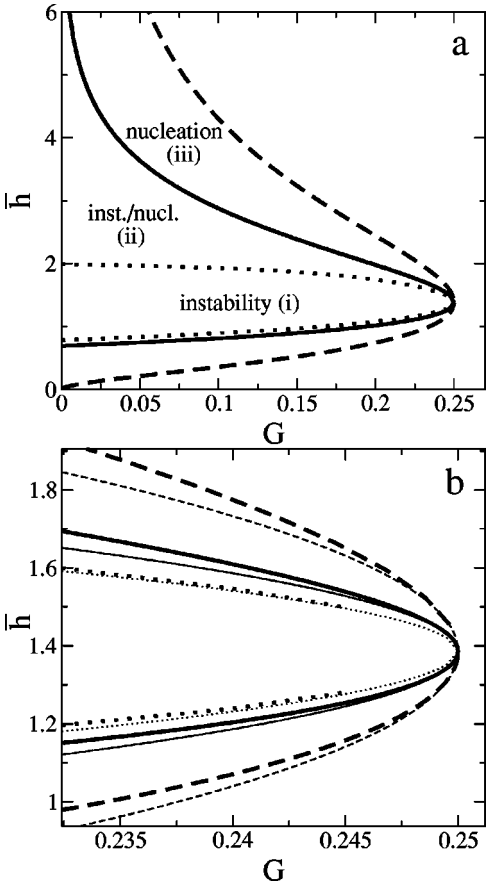

FIG. 10. The three film thickness regimes due to different types of families of stationary solutions [(i), (ii) and (iii)], as defined in the main text, shown in the parameter plane $(G,\bar{h})$. Dashed lines separate stable films from range (iii), solid lines separate range (iii) from range (ii), and dotted lines separate range (ii) from range (i). Shown is in (a) the full relevant parameter plane, and in (b) a zoom close to the critical point at $[0.25,\ln(4)]$. In (b) the thick lines show the numerical values of the borders as in (a), and the thin lines represent the respective analytical approximations as obtained in the Appendix.

V. STABILITY OF PERIODIC SOLUTIONS

Let us assess the linear stability of the periodic solutions obtained in Sec. IV by linearizing the full time dependent equation (7) around the periodic solutions, $h_0(x)$. Taking for the disturbance the ansatz $h(x)=h_0(x)+\epsilon h_1(x)e^{\beta t}$ gives the $O(\epsilon)$ equation

$$\begin{aligned}\beta h_1=&\{[3q^2(h_{0x}f_{hh}-h_{0xxx})]_x+(q^3h_{0x}f_{hhh})_x\}h_1\\&+[2q^3h_{0x}f_{hhh}+3q^2(2h_{0x}f_{hh}-h_{0xxx})]h_{1x}\\&+q^3f_{hh}h_{1xx}-3q^2h_{0x}h_{1xxx}-q^3h_{1xxxx},\end{aligned}\tag{26}$$

where $q=h_0(x)-\ln a$ and all derivatives of f are functions of the periodic solution $h_0(x)$. For a disturbed flat film, Eq. (26) reduces to Eq. (15).

To solve Eq. (26) numerically, we discretize it by expressing the derivatives of $h_1[i]$ at a point i as a linear combina-

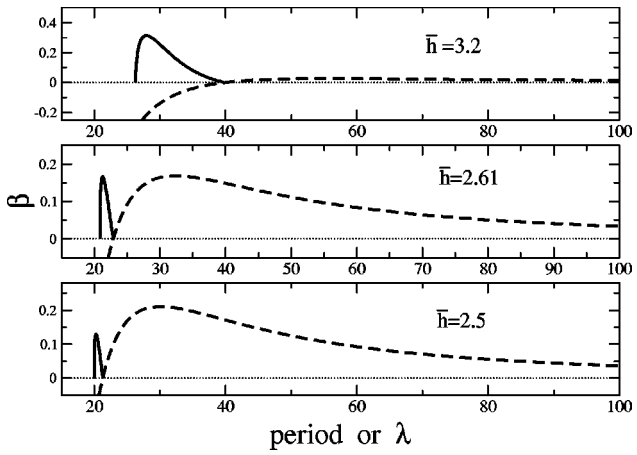

FIG. 11. Dependence of the linear growth rate β on the period for nucleation solutions (solid lines) and on wavelength λ for flat film solutions (dashed lines) for different values of $\bar{h}$ and $G=0.05$.

tion of $h_1[n]$ where $i-2\leqslant n\leqslant i+2$. Using periodic boundary conditions, this yields the algebraic eigenvalue problem

$$\beta h_1+\mathcal{L}(h_0,h_{0x},h_{0xx},h_{0xxx},h_{0xxxx},f_h,f_{hh},f_{hhh})h_1=0, \tag{27}$$

where $\mathcal{L}$ is a linear operator determined by the periodic solution, h_0. We search for the largest eigenvalues (i.e., growth rates) β, and the corresponding eigenvectors h_1 (i.e., disturbances).

For a given $\bar{h}$ we first calculate the linear growth rates of disturbances to the solutions of the terminating branch of nucleation solutions in the mixed range (ii), taking one period of the respective solutions as the unit of the stability analysis. The obtained linear growth rates we compare to the linear growth rates for the flat film modes at film thickness $\bar{h}$ obtained with Eq. (15). Taking, for example, $G=0.05$, Fig. 11 shows that the growth rate for the nucleation solution depends nonmonotonically on its period. The maximum of this dispersion relation can be larger or smaller than the maximum of the dispersion relation of the linear modes for the corresponding flat film. This gives us evidence that within the newly found mixed regime, depending on film thickness, we encounter a generically different behavior in the time evolution. However, before we further support this statement by integrating the time evolution equation, we use this finding to delineate a separation between nucleation-dominated and instability-dominated behavior within the linearly unstable thickness range. We define this border to be at the film thickness where the maximum growth rates of the flat film mode, given by Eq. (20), and that of the periodic nucleation solution are equal as in Fig. 11. The numerically calculated values are plotted in Figs. 12(a) and 12(b), for $h>h_c$ and $h<h_c$, respectively.

We further confirm the stability of the lower solution branch, upon which we already concluded by considering its energy. The always negative growth rate of disturbances, taking one period of the stationary solution as the unit for the stability analysis, is shown in Fig. 13(a). The minimum points to the most stable solution, i.e., a solution that relaxes faster than others to its stationary shape when perturbed. Note that its period is not correlated to the wavelength of the fastest flat film mode. However, studying the linear stability of the lower solution branch, taking multiples of the period of the stationary solution as unit for the stability analysis, gives a positive growth rate for disturbances representing coarse graining. The growth rates for the case where the unit is twice the period of the analyzed solution are plotted in Fig. 13(b). The ongoing coarse graining leads to a long-time evolution that goes toward solutions with larger period. We will not dwell on this issue here.

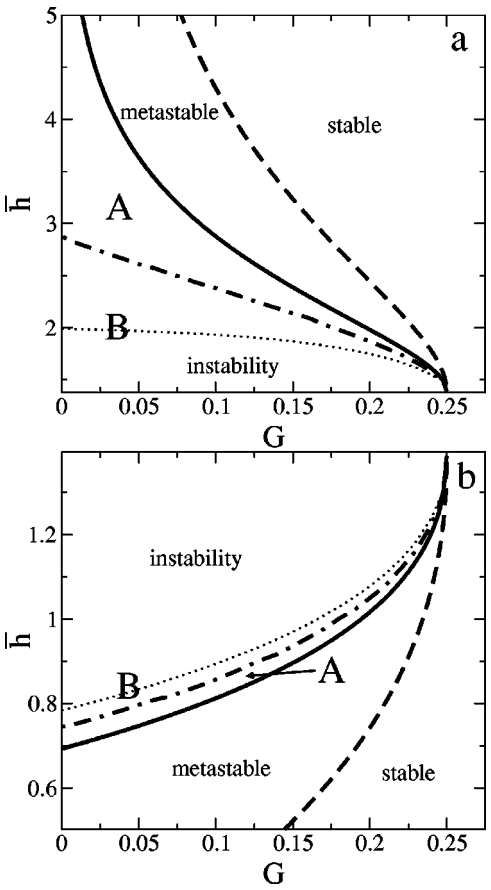

FIG. 12. The different rupture regimes are shown within the parameter plane $(G,\bar{h})$ for (a) $\bar{h}>h_c$ and (b) $\bar{h}<h_c$. The linearly unstable range lying to the left of the solid line is divided by the dot-dashed line in the nucleation-dominated subrange denoted *A* and the instability-dominated subrange denoted *B*. The dotted line shows the location where the branch of nucleation solutions ceases to exist.

VI. TIME EVOLUTION

Taking the linear stability results for the stationary solutions in their exact mathematical sense, we can only state that, for linearly unstable flat films, there exists a thickness range—the nucleation-dominated range—where some periodic finite perturbations corresponding to certain nucleation solutions yield linear growth rates much larger than the lin-

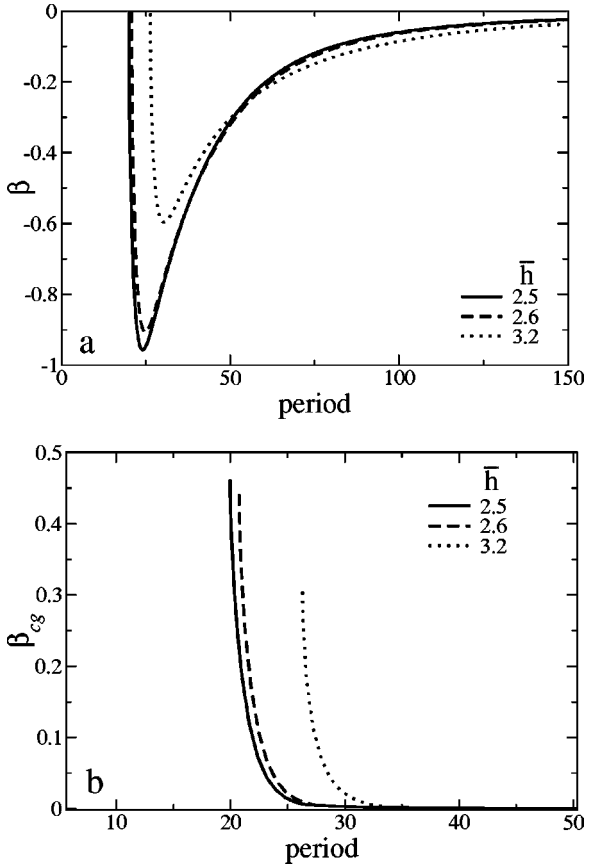

FIG. 13. Linear stability results for the lower branch of periodic solutions for different $\bar{h}$ at fixed $G=0.05$. The units for the stability analysis are (a) one period and (b) two periods of the stationary solution. (b) shows their instability with respect to coarse graining.

ear growth rate of the fastest flat film mode. However, we take this result only as a hint on the local structure of the flow, $\partial_t h$, close to these nucleation solutions and hence we assume that in the nucleation-dominated range, local finite perturbations of a lateral extension smaller than the critical wavelength for flat film modes λ_c have a crucial influence on the structure formation, whereas they have a negligible role in the instability-dominated range. To show this we integrate the time dependent equation (7) for a system of size $n\lambda_m$, taking as an initial condition a flat film with a localized disturbance,

$$h_{init}=\bar{h}\left[1-d\cosh\left(\frac{x}{w\lambda_m}\right)^{-2}\right], \tag{28}$$

with periodic boundary conditions. $n>1$ is an integer, λ_m is the wavelength of the fastest growing flat film mode for $\bar{h}$, d is the maximum disturbance depth in units of $\bar{h}$, and w is a measure of its width in terms of λ_m.

The results of the time evolution for many different initial disturbances and mean thicknesses permit one to sustain the assumption given above, namely, the qualitative distinction of the two thickness regions within the linearly unstable thickness range as introduced in Sec. V and shown in Fig. 12.

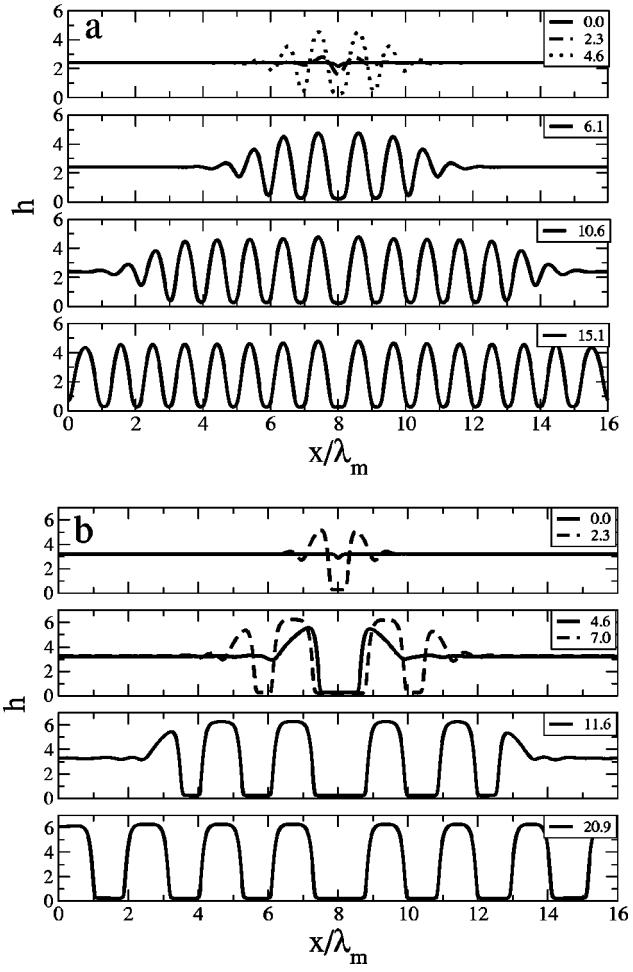

FIG. 14. Short-time evolution for a localized disturbance with $d=0.1$ and $w=0.2$ at $G=0.05$. (a) Instability dominated at $\bar{h}=2.4$. (b) Nucleation dominated at $\bar{h}=3.2$. The coordinate x is shown in units of the wavelength corresponding to the fastest growing linear mode, λ_m. Insets give the time in units of the growth time $\tau_m=1/\beta_m$ of the same mode.

(A) Nucleation-dominated region. The initial disturbance grows downward, forming a hole with rims at its two sides. This hole then expands laterally. Eventually, the thickness depressions at the outer bases of the rims lead to secondary nucleation events. An example of this type of evolution is shown in Fig. 14(b). The final, short-time structure (before coarse graining sets in) is a set of holes with distances unrelated to λ_m [last picture of Fig. 14(b)]. The details of the process and the resulting spatial structure depend strongly on the width and depth of the initial disturbance, as can be seen in the Fourier spectra of a set of final structures [Fig. 15(b)] or in the evolution of the spatially averaged energy, resulting in different values for the final short-time structure [shown in Fig. 16(b)]. Analogous differences are seen in the evolution of the spatially averaged second moment of the film thickness (not shown). Note that in the evolution of the energy one can clearly distinguish the individual secondary nucleation events, giving the process a steplike character. The individual nucleation events seem to show power law behavior. Further simulations show that the secondary nucleation be-

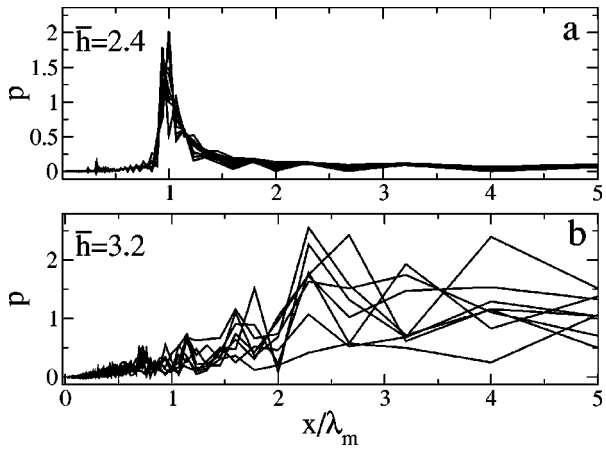

FIG. 15. Fourier transforms of the final short-time, spatial patterns for (a) $\bar{h}=2.4$ at time $t/\tau_m=17.2$, and (b) $\bar{h}=3.2$ at time $t/\tau_m=20.9$. Both figures show results for a number of runs for different depths ($d=0.1\ldots0.4$) and widths ($w=0.1\ldots0.4$) of the initial disturbance for $G=0.05$. The x axis is as in Fig. 14.

comes less important for mean film thicknesses closer to the border of the linearly unstable range.

(B) Instability-dominated region. The initial disturbance starts to grow downwards as in (A) but from the beginning provokes the growth of undulations on its both sides. These undulations have the wavelength of the most unstable flat film mode, and extend laterally with approximately constant velocity. This process gives the impression of a growing wave packet. An example is shown in Fig. 14(a). The final short-time structure is a nearly periodic set of holes, whatever the width and depth of the initial perturbation may be, as shown in the Fourier spectra of a set of final structures in Fig. 15(a). Studying the evolution of the energy [Fig. 16(a)], we see that only the evolution at its very early stage depends on the details of the initial perturbation. Then the evolution is

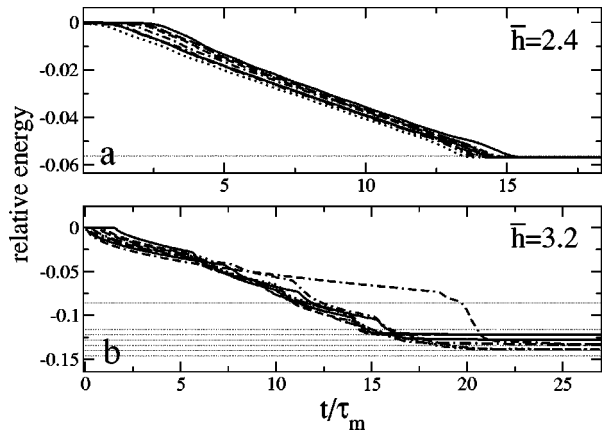

FIG. 16. Average energies subtracted from the corresponding flat film energies are plotted for the short-time evolution at (a) $\bar{h}=2.4$ and (b) $\bar{h}=3.2$. A number of runs is shown as in Fig. 15 (thick lines, different linestyles). The thin dotted lines represent the energy for stationary solutions with periods (a) $p=\lambda_m$ and (b) $p=\lambda_m, 16\lambda_m/11, 16\lambda_m/10, 16\lambda_m/9, 16\lambda_m/8, 16\lambda_m/7$, and $16\lambda_m/6$ (from above).

nearly identical, albeit slightly shifted in time. The approximate linearity of these curves shows that the lateral extension of the instability is a smooth process of constant velocity. In contrast to (*A*), different perturbations result in the same energy for the final short-time structure corresponding to the energy of the stationary solution of period, *p*, equal to to the wavelength of the fastest flat film mode λ_m. The spatially averaged second moment of the film thickness shows an analogous behavior.

The dramatic difference found in the time evolution confirms the above introduced separation in two experimentally distinguishable subranges—the nucleation-dominated subrange (*A*) and the instability-dominated subrange (*B*)—within the linearly unstable range. Further simulations for a range of mean film thicknesses at different parameters *G* show that the transition between the two subranges occurs roughly at the dot-dashed line in Fig. 12, as defined in Sec. V. Being a bit apart from the transition line, the size of the initial disturbance has no influence on *which* of the two scenario occurs, but only on *how* it occurs. However, in the transition region the size of the inital disturbance does strongly influence *which* process occurs. This is due to the fact that, in situations close to equal fastest linear growth rates for flat film modes and periodic nucleation solutions [as in Fig. 11(b)] only part of the periodic solutions grow faster than the fastest flat film mode. Therefore, between (*A*) and (*B*), depending on the depth and width of the initial disturbance, one finds behavior corresponding to (*A*) or (*B*) or combinations of structures caused by secondary nucleation and growth of the fastest flat film mode. In the latter case the details depend also on system size.

VII. DISCUSSION AND CONCLUSION

We have analyzed the evolution of a thin liquid film under the influence of the disjoining pressure that arises in the combination of diffuse interface theory with thin film hydrodynamics [33]. First we determined the stable, metastable, and linearly unstable thickness ranges according to the values of the control parameter *G*, and discussed the flat film solutions, and bifurcations when parameters change values. Then, we have obtained the families of stationary periodic and localized solutions and have assessed their linear stability. In the metastable film thickness range we identified periodic and localized nucleation solutions that separate decaying and growing finite disturbances. A second branch consists of periodic solutions that are linearly stable, taking their periods as units for the stability analysis. However, they are unstable if multiples of their period are taken as units for the stability analysis (coarse graining).

In the linearly unstable film thickness range we have distinguished two subranges showing qualitatively different behaviors: (A) a nucleation-dominated region and (B) an instability-dominated region. In the nucleation-dominated subrange initial small-scale finite disturbances are crucial for the final structure, and the linearly unstable flat film modes are too slow to act. In the instability-dominated sub-range the situation is the opposite. The fastest flat film wavelength determines the structure formation, and finite disturbances

have negligible influence on the process. This was confirmed by a direct integration of the time evolution equation (7). Despite the restriction to two-dimensional geometry, we believe this distinction is also valid for the more realistic three-dimensional geometry.

The results obtained are also valid for other, formally similar disjoining pressures that describe short-range destabilizing and long-range stabilizing interactions such as the widely used pressure that combines destabilizing polar and stabilizing apolar molecular interactions (case IV in Refs. [26,28,30,31,35], and also used in Ref. [11,14]). Such a disjoining pressure can be accommodated in our theory by replacing the unscaled function $\partial_h f$ resulting from diffuse interface theory [Eq. (2)] with the negative of the disjoining pressure from Ref. [26] (case IV) and introducing an adapted scaling. Then calculations as performed here yield a similar difference between nucleation-dominated and instability-dominated subranges within the linearly unstable thickness range [36]. The results for this disjoining pressure complement Ref. [28] (case IV), where they studied the time evolution of finite amplitude sinusoidal perturbations with wavelengths larger than the critical wavelength of the linear flat film mode, λ_c. They compared this nonlinear time evolution to the extrapolated behavior of the corresponding linear modes. In contrast, we focus on small scale disturbances (defects) with lateral extensions smaller than λ_c. Also, we compare, on the one hand, only linear growth rates of flat film modes and nucleation solutions (Fig. 11), and on the other hand only the nonlinear evolutions of finite disturbances and flat film modes (Figs. 14–16). However, in addition to the qualitatively similar main result here and in Ref. [36], namely, the existence of the subranges (*A*) and (*B*), the different disjoining pressures cause important details to differ as can best be seen by comparing the final parameter plane here (Figs. 5 and 12) with Fig. 4 of Ref. [36]. Increasing the strength of the destabilizing short-range interaction in Ref. [36] causes even very thick films to be only metastable and not absolutely stable. Here, on the contrary, there exists an upper border for the metastable range for all $G \neq 0$. In addition, in Ref. [36] for vanishing stabilizing interaction, the entire thickness range is dominated by nucleation indicated by the border between (*A*) and (*B*), approaching $\bar{h}=0$, whereas here no such dramatical change occurs, the border between (*A*) and (*B*) approaches a finite value of $\bar{h}$ as $G \rightarrow 0$. The behavior in Ref. [36] is caused by the divergence of the disjoining pressure for vanishing film thickness. Our results, especially the description of the families of periodic nucleation solutions, can also be used to extend the findings of single critical droplets and holes for first-order wetting transitions [45,46] toward finite periods.

Experimental systems with formally similar disjoining pressures were investigated in Refs. [14,48]. The experiments of Refs. [4,9,12] can also be discussed in our framework if one includes gravitation as a long-range stabilizing interaction, competing with the destabilizing apolar interaction (the limiting case of very small G). In Refs. [14,48] the different patterns observed were explained by the distinction of thickness ranges for dewetting by nucleation and spinodal dewetting. Our results merely shift the boundary between the two regimes. This explains why in Ref. [48] the transition between their regime III (spinodal holes or ''less random nucleation'' in their jargon) and IV (nucleated holes or ''random nucleation'') seems to be already in the upper part of the spinodal regime. Note that their random droplet regime (II) corresponds to our lower nucleation range. In the experiments of Refs. [4,9], the authors agreed in describing the situation as linearly unstable. On the one hand, the process is seen as spinodal dewetting based on the dependence of the hole density on the film thickness [4], and on the other hand it is seen as dewetting by nucleation based on the random distribution of the holes [9]. The ambiguity is eliminated if we consider that the experiments were done with film thicknesses that correspond to the nucleation-dominated subrange within the linearly unstable range with some disturbances present that eventually determine the dewetting process. The spinodal dewetting could only be seen in a small thickness range, or in situations with little or no finite disturbances or defects in the film. Three-dimensional analyses of the dewetting process, as done in Refs. [30,32] with initial conditions like those used here in Sec. VI are expected to support our view by studying the competing influence of finite disturbances and the linear instability of the flat film in a realistic geometry.

The question of nucleation in the linearly unstable thickness range was also raised in systems exhibiting spinodal decomposition, where the thickness in our study is replaced by the concentration of one component. Different aspects discussed here were described for equations similar to our analytic limiting case [Eq. (A7)]. In Refs. [38,39] the free energy has an additional cubic term, and Ref. [40] uses a general quartic expression. Although their solutions are different, certain general features are found in all the systems. The study in Ref. [38] of the stationary periodic concentration profiles and their parameter dependence led to a qualitative discrimination analogous to our distinction in three different families of solutions (i), (ii), and (iii) in Sec. IV but without determining the boundary between (i) and (ii). They identify the positive-energy branch within the metastable range as periodic nucleation-type solutions [38], and suggest that ''the phase separation in the deep spinodal region, may be distinguishable, perhaps more nearly periodic or 'spinodal,' than in the rest of the spinodal region'' [39]. The latter corresponds to our distinction between instability-dominated and nucleation-dominated subranges within the linearly unstable thickness range.

Reference [40] focused on the stability of periodic concentration profiles to perturbations of equal period, aiming at a characterization of the short-time behavior of multilayer systems. The authors found different solution types that correspond to the periodic nucleation solutions and stable periodic solutions described here. They established concentration (film thickness) ranges for the absolute stability, metastability, and linear instability of different solution types at fixed periods, comparing the energy of homogeneous solutions (flat film) and periodic solutions. Their analysis corresponds to part of our discussion of Fig. 7 in Sec. IV, especially in (ii) and (iii). From these analogies we conclude that the findings

presented here can also account for phenomena occurring in spinodal decomposition. In particular, the conjecture of a highly disturbance-dependent system behavior in a subregion of the spinodal region in spinodal decomposition [39] can be made precise using the quantitative description of the transition between nucleation-dominated and instability-dominated subranges within the linearly unstable thickness range introduced here.

ACKNOWLEDGMENTS

This research was supported by the European Union under ICOPAC Grant No. HPRN-CT-2000-00136, by the German Academic Exchange Board (DAAD) under Grant No. D/98/14745, and by the Spanish Ministry of Science and Technology under Grant No. PB 96-599.

APPENDIX A: ANALYTICAL SOLUTIONS CLOSE TO BIFURCATIONS

Close to the bifurcation lines one can approximately obtain the solutions analytically. These results are used to cross check the numerical results.

1. Close to the linear instability line

The transition line between the metastable and the linearly unstable film thickness range in the (G,h) plane corresponds to the crossing of two fixed points of Eq. (13), as shown in Fig. 3(b) for fixed G. The line in the phase plane is characterized by $\partial_{hh}f(h)=0$, allowing one to approximate Eq. (13) close to this line. We introduce the local variables $h_0=h_0^*+\mu$ and $h=h_0^*+\epsilon(x)$ where h_0^* is the film thickness on the bifurcation line and $O(\mu)\approx O(\epsilon(x))\ll 1$. Writing Eq. (13) to $O(\mu^2)$ gives

$$0=\partial_{xx}\epsilon-\tfrac{1}{2}\,\partial_{hhh}f|_{h_0^*}(\epsilon^2-\mu^2), \tag{A1}$$

that can be integrated. The choice of the integration constant $\overline{C_2}$ permits one to obtain the homoclinic solutions ($\overline{C_2}=0$)

$$\epsilon=\mu\left(3\tanh^2\left[\frac{1}{2}\sqrt{\mu f_3}(x-x_0)\right]-2\right) \tag{A2}$$

or the periodic solutions [$\overline{C_2}=\frac{1}{2}f_3(\epsilon_{max}^3/3-\mu^2\epsilon_{max})$]

$$\epsilon=c_3+(c_2-c_3)\,\mathrm{sn}^2\left[\frac{\sqrt{f_3}\sqrt{c_1-c_3}(x-x_0)}{2\sqrt{3}},\frac{c_2-c_3}{c_1-c_3}\right], \tag{A3}$$

where $\mathrm{sn}[u,k]$ is the Jacobi sine amplitude, and f_3 stands for $\partial_{hhh}f|_{h_0^*}$. Close to the upper instability line in the phase plane (related to hole solutions) c_3 is the minimal thickness ϵ_{min}, c_2 is the maximal thickness ϵ_{max}, and $c_1>c_2$ has no obvious physical meaning. Given $\epsilon_{max}=c_2$, the other ϵ_i are given by

$$c_{1/3}=\frac{1}{2}(-c_2\pm\sqrt{3}\sqrt{4\mu^2-c_2^2}), \tag{A4}$$

where the positive sign gives $\epsilon_{min}=c_3$.

Looking for periodic solutions close to the lower instability line (related to drop solutions), we identify the constants as follows: c_2 is the given $\epsilon_{min.}$ $c_3=\epsilon_{max}$ and $c_1<c_2$ are interchanged with respect to above. The Jacobi elliptic function $\mathrm{sn}[u,k]$ gives periodic solutions for $k\neq 1$. For $k=(c_2-c_3)/(c_1-c_3)=1$, it goes over to the homoclinic solution given by Eq. (A2). The period of the solutions is given by

$$p(\mu,c_2)=\frac{4\sqrt{3}}{\sqrt{f_3}\sqrt{c_1-c_3}}K\left[\frac{c_2-c_3}{c_1-c_3}\right], \tag{A5}$$

and the mean film thickness by

$$\overline{\epsilon}(\mu,c_2)=c_3+(c_1-c_3)\times\left(1-E\left[\frac{c_2-c_3}{c_1-c_3}\right]\Big/K\left[\frac{c_2-c_3}{c_1-c_3}\right]\right), \tag{A6}$$

where $K[k]$ and $E[k]$ are the complete elliptic integrals of the first and second kinds, respectively.

2. Close to the critical point

Close to the critical point ($G_c=1/4, h_c=\ln 4$), we introduce $h_0=h_c+\mu$, $h(x)=h_c+\epsilon(x)$ and $G=G_c+g$ with $O(\mu)\approx O(\epsilon(x))\approx O(g)\ll 1$. We are interested in the range of negative values of g. Writing Eq. (13) to $\mathrm{O}(\epsilon^3)$, thereby taking into account that $\partial_h f(h_c)=C_1$ and $\partial_{hh}f(h_c)=\partial_{hhh}f(h_c)=0$ (see Sec. III), gives

$$0=\partial_{xx}\epsilon-\tfrac{1}{6}\partial_{hhhh}f|_{h_c}(\epsilon^3-\mu^3)-g(\epsilon-\mu). \tag{A7}$$

Integrating Eq. (A7) twice yields the general periodic solutions

$$\epsilon=\epsilon_2+\frac{\epsilon_1-\epsilon_2}{1+a\ \mathrm{sn}^2[c(x-x_0),k]}, \tag{A8}$$

with

$$a=\frac{\epsilon_1-\epsilon_4}{\epsilon_4-\epsilon_2},\quad k=\frac{(\epsilon_2-\epsilon_3)(\epsilon_1-\epsilon_4)}{(\epsilon_1-\epsilon_3)(\epsilon_2-\epsilon_4)},$$
$$c=\frac{1}{4}\sqrt{\frac{f_4}{3}(\epsilon_1-\epsilon_3)(\epsilon_2-\epsilon_4)}, \tag{A9}$$

and the period

$$p=\frac{2}{c}K[k]. \tag{A10}$$

ϵ_4 is the value given at an extremum ϵ_m and the other ϵ_i are the roots of the cubic equation $\epsilon^3+d_1\epsilon^2+d_2\epsilon+d_3=0$ with $d_1=\epsilon_m$, $d_2=12g/f_4+\epsilon_m^2$ and $d_3=\epsilon_m^3-4\mu^3+12g\epsilon_m/f_4-24g\mu/f_4$, and f_4 stands for $\partial_{hhhh}f|_{h_c}$.

At $\epsilon_m=\mu$ and $\mu=\mu_f=\sqrt{-6g/f_4}$ the three remaining roots are $(\mu_f,-\mu_f,-\mu_f)$ and Eq. (A8) reduces to the heteroclinic or front solution

$$\epsilon = \mu_f \tanh[\mu_f (x - x_0)], \tag{A11}$$

that connects two flat films $\epsilon_{max} = \mu_f$ and $\epsilon_{min} = -\mu_f$, symmetric with h_c. The relation $\mu_f^2 + 6g/f_4 = 0$ is also an approximation close to the critical point for the border between absolutely stable and metastable flat films. To obtain the local approximation of the border between metastable and linearly unstable thickness ranges, we use the ansatz $\epsilon = \mu + \delta \exp(ikx)$ ($\delta \ll \mu$) in Eq. (A7) to obtain the relation $\mu_f^2 + 2g/f_4 = 0$.

However, calculating the border between the purely spinodal region (i) and the region where also periodic nucleation solutions exist (ii) requires some more effort. We approximate the thickness profile for small amplitudes as

$$\epsilon(x) = \mu + \alpha(A_1 \exp(ikx) + \overline{A_1} \exp(-ikx)) + \alpha^2(A_2 \exp(2ikx) + \overline{A_2} \exp(-2ikx))$$

with $\alpha \ll 1$. This is valid for periodic solutions with wave numbers k close to the critical wave number k_c, expressed by $k^2 = k_c^2(1 - r_1\alpha^2 - r_2\alpha^4)$. Introducing these relations in Eq. (A7) we project onto the modes $\exp(ikx)$ and $\exp(2ikx)$, yielding two stationary amplitude equations for the A_i. The first order in α gives k_c, the second order yields a relation between A_1 and A_2, and the third order gives the relation $r_1 = A_1^2 s(\mu, g)$, where s is some function. At the border the derivative of the wave number with respect to amplitude changes sign, i.e., $r_1 = 0$. The resulting condition $s(\mu, g) = 0$ gives the border at $\mu_f^2 + \frac{6}{5} g f_4 = 0$.

[1] H. S. Kheshgi and L. E. Scriven, Chem. Eng. Sci. **46**, 519 (1991).
[2] M. Mertig, U. Thiele, J. Bradt, D. Klemm, and W. Pompe, Appl. Phys. A: Solids Surf **66**, S565 (1998).
[3] F. Brochard-Wyart and J. Daillant, Can. J. Phys. **68**, 1084 (1989).
[4] G. Reiter, Phys. Rev. Lett. **68**, 75 (1992).
[5] E. Ruckenstein and R. Jain, J. Chem. Soc., Faraday Trans. 2 **70**, 132 (1974).
[6] R. Khanna, A. Sharma, and G. Reiter, EPJdirect **E2**, 1 (2000).
[7] C. Redon, F. Brochard-Wyart, and F. Rondelez, Phys. Rev. Lett. **66**, 715 (1991).
[8] K. Jacobs, R. Seemann, G. Schatz, and S. Herminghaus, Langmuir **14**, 4961 (1998).
[9] K. Jacobs, S. Herminghaus, and K. R. Mecke, Langmuir **14**, 965 (1998).
[10] V. S. Mitlin, J. Colloid Interface Sci. **233**, 153 (2001).
[11] N. Samid-Merzel, S. Lipson, and D. S. Tannhauser, Phys. Rev. E **57**, 2906 (1998).
[12] J. Bischof, D. Scherer, S. Herminghaus, and P. Leiderer, Phys. Rev. Lett. **77**, 1536 (1996).
[13] R. Xie, A. Karim, J. Douglas, C. Han, and R. Weiss, Phys. Rev. Lett. **81**, 1251 (1998).
[14] U. Thiele, M. Mertig, and W. Pompe, Phys. Rev. Lett. **80**, 2869 (1998).
[15] G. Reiter, A. Sharma, A. Casoli, M.-O. David, R. Khanna, and P. Auroy, Langmuir **15**, 2551 (1999).
[16] G. Reiter, Langmuir **9**, 1344 (1993).
[17] A. Oron, S. H. Davis, and S. G. Bankoff, Rev. Mod. Phys. **69**, 931 (1997).
[18] J. W. Cahn and J. W. Hillard, J. Chem. Phys. **28**, 258 (1958).
[19] V. S. Mitlin, J. Colloid Interface Sci. **156**, 491 (1993).
[20] B. V. Derjaguin, Zh. Fiz. Khim. **14**, 137 (1940).
[21] B. V. Derjaguin, N. V. Churaev, and V. M. Muller, *Surface Forces* (Consultants Bureau, New York, 1987).
[22] G. F. Teletzke, H. T. Davis, and L. E. Scriven, Rev. Phys. Appl. **23**, 989 (1988).
[23] R. J. Hunter, *Foundation of Colloid Science* (Clarendon Press, Oxford, 1992), Vol. 1.
[24] J. N. Israelachvili, *Intermolecular and Surface Forces* (Academic Press, London, 1992).
[25] V. M. Starov, Adv. Colloid Interface Sci. **39**, 147 (1992).
[26] A. Sharma, Langmuir **9**, 861 (1993).
[27] A. Sharma, J. Colloid Interface Sci. **156**, 96 (1993).
[28] A. Sharma and A. T. Jammel, J. Colloid Interface Sci. **161**, 190 (1993).
[29] A. T. Jammel and A. Sharma, J. Colloid Interface Sci. **164**, 416 (1994).
[30] A. Sharma and R. Khanna, Phys. Rev. Lett. **81**, 3463 (1998).
[31] A. Sharma and R. Khanna, J. Chem. Phys. **110**, 4929 (1999).
[32] A. Oron, Phys. Rev. Lett. **85**, 2108 (2000).
[33] L. M. Pismen and Y. Pomeau, Phys. Rev. E **62**, 2480 (2000).
[34] P. G. de Gennes, Rev. Mod. Phys. **57**, 827 (1985).
[35] A. Sharma, Langmuir **9**, 3580 (1993).
[36] U. Thiele, M. G. Velarde, and K. Neuffer, Phys. Rev. Lett. **87**, 016104 (2001).
[37] J. Langer, Ann. Phys. (N.Y.) **65**, 53 (1971).
[38] A. Novick-Cohen and L. A. Segel, Physica D **10**, 277 (1984).
[39] A. Novick-Cohen, J. Stat. Phys. **38**, 707 (1985).
[40] M. Hentschel, M. Bobeth, G. Diener, and W. Pompe, Thin Solid Films **354**, 267 (1999).
[41] A. Sharma and E. Ruckenstein, J. Colloid Interface Sci. **113**, 456 (1986).
[42] A. Oron and P. Rosenau, J. Phys. II **2**, 361 (1992).
[43] V. S. Mitlin, J. Colloid Interface Sci. **227**, 371 (2000).
[44] h_m^u contains no $O(1)$ term, as can be seen in the next order approximation, giving $h_m^d = \sqrt{G/2}(1 + \frac{3}{8}\sqrt{2}\sqrt{G}) + O(G^{3/2})$ and $h_m^u = \sqrt{2/G} - (\sqrt{2}/16)\sqrt{G} + \frac{21}{128} G + O(G^{3/2})$.
[45] R. Bausch and R. Blossey, Phys. Rev. E **48**, 1131 (1993).
[46] R. Bausch, R. Blossey, and M. Burschka, J. Phys. A **27**, 1405 (1994).
[47] E. Doedel, A. Champneys, T. Fairfrieve, Y. Kuznetsov, B. Sandstede, and X. Wang, *AUTO97: Continuation and Bifurcation Software for Ordinary Differential Equations* (Concordia University Press, Montreal, 1997).
[48] H. I. Kim, C. M. Mate, K. A. Hannibal, and S. S. Perry, Phys. Rev. Lett. **82**, 3496 (1999).